Fuel 158 (2015) 999–1005

Contents lists available at ScienceDirect

Fuel

journal homepage: www.elsevier.com/locate/fuel

# Catalytic steam reforming of volatiles released via pyrolysis of wood sawdust for hydrogen-rich gas production on Fe–Zn/$Al_2O_3$ nanocatalysts

Fangyuan Chen [a,c], Chunfei Wu [b,d,*], Lisha Dong [a], Fangzhu Jin [a], Paul T. Williams [b,*], Jun Huang [a,*]

[a] Laboratory for Catalysis Engineering, School of Chemical and Bimolecular Engineering, The University of Sydney, NSW 2006, Australia
[b] Energy Research Institute, University of Leeds, Leeds LS2 9JT, UK
[c] School of Environmental Science & Engineering, Kunming University of Science & Technology, Kunming 650038, PR China
[d] School of Engineering, University of Hull, Hull HU6 7RX, UK

## HIGHLIGHTS

- Hydrogen is produced directly from wood sawdust gasification.
- Cost effective catalysts based on iron have been studied.
- Fe–Zn/$Al_2O_3$ with a Zn/Al ratio of 1:1 showed the highest $H_2$ production.
- Fe spinels in the catalyst are important for resistance of coke formation.
- Zn promoted Fe nanocatalysts are promising for biomass gasification.

## ARTICLE INFO

*Article history:*
Received 2 October 2014
Received in revised form 27 March 2015
Accepted 19 May 2015
Available online 1 June 2015

*Keywords:*
Biomass
Catalyst
Reforming
Hydrogen
Syngas
Nanocatalysts

## ABSTRACT

Thermo-chemical processing of biomass is a promising alternative to produce renewable hydrogen as a clean fuel or renewable syngas for a sustainable chemical industry. However, the fast deactivation of catalysts due to coke formation and sintering limits the application of catalytic thermo-chemical processing in the emerging bio-refining industry. In this research, Fe–Zn/$Al_2O_3$ nanocatalysts have been prepared for the production of hydrogen through pyrolysis catalytic reforming of wood sawdust. Through characterization, it was found that Fe and Zn were well distributed on the surface with a narrow particle size. During the reactions, the yield of hydrogen increased with the increase of Zn content, as Zn is an efficient metal promoter for enhancing the performance of the Fe active site in the reaction. The 20% Fe/$Al_2O_3$ catalyst with Zn/Al ratio of 1:1 showed the best performance in the process in relation to the hydrogen production and resistance to coke formation on the surface of the reacted catalyst. All the catalysts showed ultra-high stability during the process and nearly no sintering were observed on the used catalysts. Therefore, the nanocatalysts prepared in this work from natural-abundant and low-cost metals have promising catalytic properties (high metal dispersion and stability) to produce $H_2$-rich syngas with optimal $H_2$/CO ratio from the thermo-chemical processing of biomass.



## 1. Introduction

Hydrogen is one of the few long-term sustainable clean energy carriers as it emits only water vapor as a by-product during the combustion and oxidation process [1–3]. However, hydrogen production can be environmentally friendly only if the resource used to extract hydrogen is carbon neutral [4]. Biomass is one of the most abundant forms of carbon neutral resources, and biomass gasification is a promising alternative to produce renewable hydrogen as a clean fuel or renewable syngas ($CO_2$, CO, $H_2$) for a sustainable chemical industry [5–9]. Of all the thermo-chemical processes, however, biomass gasification still suffers from lower hydrogen production and higher tar formation compared to the process using fossil fuels. Recently, biomass catalytic gasification has been shown to greatly increase hydrogen yield and decrease tar formation. Dolomite, $CeO_2$/$SiO_2$ supported Ni, Pt, Pd, Ru and alkaline metal oxides have been reported to be effective in tar reduction and conversion efficiency [5]. However, one significant challenge for catalytic gasification is the fast deactivation of

* Corresponding authors at: Energy Research Institute, University of Leeds, Leeds LS2 9JT, UK. Tel.: +44 1482466464 (C. Wu). Tel.: +44 113 3432504 (P.T. Williams). The University of Sydney, Sydney, NSW 2006, Australia. Tel.: +61 2 9351 7483 (J. Huang).
*E-mail addresses:* c.wu@hull.ac.uk (C. Wu), p.t.williams@leeds.ac.uk (P.T. Williams), jun.huang@sydney.edu.au (J. Huang).

http://dx.doi.org/10.1016/j.fuel.2015.05.040
0016-2361/

catalysts due to coke formation and sintering, which limits the application of catalytic gasification in the emerging bio-refining industry [10–12]. Therefore, developing highly stable catalysts with satisfactory catalytic properties are highly desired for biomass gasification.

It is widely accepted that catalyst stability and activity are based on its physical structure and chemical composition. For supported metal catalysts in biomass gasification, many synthesis methods have been reported to control the size of nanoparticles and increase the dispersion of active metals to enhance the activity of catalysts. Moreover, the activity and stability can be further improved after using various supports and promoters to generate the support-metal interaction on catalysts. For example, a mixture of MgO or CaO with alumina support could strongly enhance the interaction between support and surface atoms of metal particles, which could strongly stabilize the metal particles to block their sintering and also enhance the metal activity due to the electron transfer between support and surface [13–17]. Recently, introducing ZnO to the support was reported to achieve high catalytic performance in methanol reforming and methyl-benzoate hydrogenation [18–20]. Lu et al. found that the catalyst of ZnO supported on $\gamma$-$Al_2O_3$ has a higher activity than ZnO or ZnO supported on $SiO_2$, $\beta$-Zeolite, and MCM-41 [20]. Interestingly, it was observed that ZnO could cover the surface acidity of the alumina support and further enhance the reducibility of supported metal particles [21–24]. Not only for better metal dispersion and size control [25], the strong interaction between ZnO and metal particles could also prevent sintering and catalytic poisoning under operating conditions [26,27].

For potential industrial application, the catalysts based on expensive noble metals such as Pt and Pd have been replaced by naturally abundant and low-cost transition metals such as Ni and Fe [28–32]. Unlike popular Ni catalysts used in catalytic gasification and reforming, there are only limited research reports related to Fe catalysts in biomass gasification due to its relatively low catalytic activity. However, Fe was believed to be catalytically active for reducing heavy hydrocarbons in the gas product during the thermo-chemical process [33–39]. It has also been adopted as a stable and active catalyst for the water–gas shift reaction (WGSR) [40]. In this study, therefore, Fe catalysts on $ZnO/Al_2O_3$ supports have been prepared by a co-precipitation method. The effect of Zn for the catalytic behavior of the catalyst, especially activity and carbon deposition, were investigated for the pyrolysis catalytic steam reforming of wood sawdust using a two-stage reaction system.

## 2. Experimental

### 2.1. Materials

Wood sawdust was used in this work as raw biomass with a size less than 0.2 mm. The physical properties of the wood sawdust are reported in our previous work [3]. The catalysts were prepared by a co-precipitation method with and initial Fe-loading mole ratio of 20 mol%. Fe $(NO_3)_3{\cdot}6H_2O(\geqslant 99\%)$, $Zn(NO_3)_3{\cdot}6H_2O(\geqslant 99\%)$, $Al_2(NO_3)_3{\cdot}9H_2O(\geqslant 99\%)$ were purchased from Sigma–Aldrich. Precursors with the desired Fe–$ZnO/Al_2O_3$ ratios were prepared by dissolving a certain amount of metal salts in deionized water. After the precipitation, the suspension was aged under agitation for an hour and then filtered under vacuum. The filter cake obtained was rinsed with deionzed water several times followed by drying at 80 °C over night. The solid products were calcined at 800 °C for 4 h with a heating rate of 1 $min^{-1}$ in static air.

### 2.2. Pyrolysis/catalytic steam reforming process

Pyrolysis/catalytic steam reforming was carried out with a fixed bed, two-stage reaction system as shown in Fig. 1. There are two stages in the reaction system, pyrolysis of biomass was performed in the first reaction stage, the derived pyrolysis vapors were catalytic steam reformed in the second stage. The two stages were externally electrically heated with separate temperature controllers. During the experiment, $N_2$ (80 ml $min^{-1}$) was used as carrier gas. 0.5 g of biomass was placed inside a crucible and held in the first pyrolysis reactor and 0.25 g of sand/catalyst was placed in the second reactor. The temperature of the second reactor was initially heated to the set point (800 °C). Then the first reactor was heated to the pyrolysis temperature (500 °C) at a heating rate of 40 $min^{-1}$ and kept at that temperature for 30 min. Water for steam reaction was injected between the two reactors with an injection rate of 0.05 g $min^{-1}$ when the temperature of the pyrolysis reactor reached 150 °C, while carrier gas $N_2$ was used during the whole experiment. The products from the pyrolysis/catalytic steam reforming were cooled using air and dry ice to collect the condensed liquid. It should be noted that tar compounds in the liquid product were not analyzed, since gas and hydrogen product were the main focus of this work. The non-condensed gases were collected using a Tedlar™ gas sample bag, and analyzed off-line using packed column gas chromatography (GC). The amounts of injected water and the condensed liquid were calculated by weighing the syringe and condensers before and after the experiments, respectively. Experiments were repeated to ensure the reliability of the results.

### 2.3. Gas analysis and catalyst characterization

Non-condensed gases collected in the Tedlar™ gas sample bag were analyzed off-line by GC. $H_2$, CO and $N_2$ were analyzed with

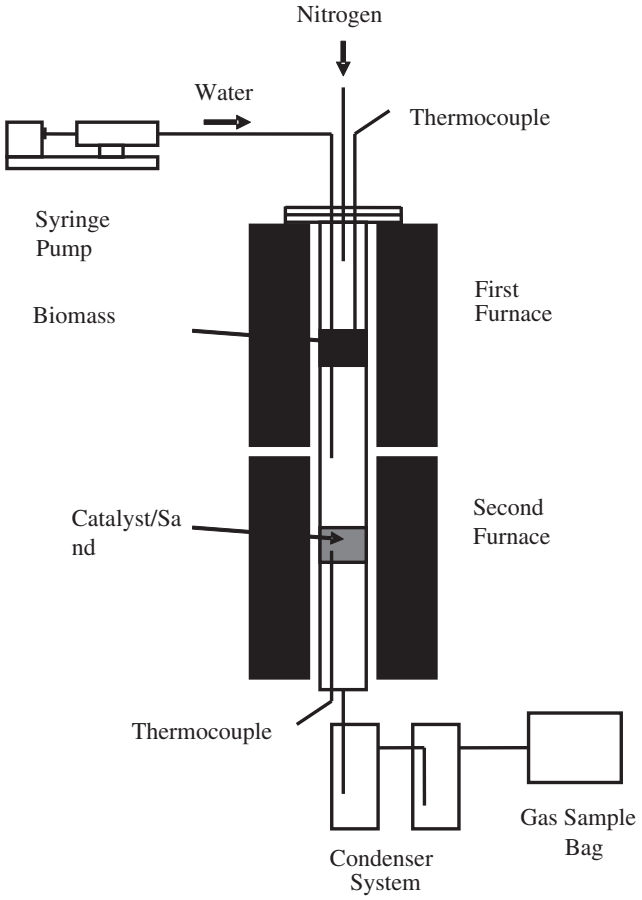


**Fig. 1.** Schematic diagram of the reaction system.

a Varian 3380 GC on a 60–80 mesh molecular sieve column with argon carrier gas, while $CO_2$ was analyzed by another Varian 3380 GC on a HayeSep 80–100 mesh column with argon carrier gas. $C_1$–$C_4$ hydrocarbons were analyzed using a Varian 3380 gas chromatograph with a flame ionisation detector, with an 80–100 mesh HayeSep column and nitrogen carrier gas. Quantification of the gas products, including $H_2$, CO, $CO_2$, $CH_4$ and $C_2$–$C_4$ hydrocarbons were obtained using the $N_2$ carrier gas with its fixed flow rate as the internal standard. During the discussion in this work, gas composition is presented excluding $N_2$.

BET surface area of the fresh catalyst was analyzed by $N_2$ adsorption and desorption isotherms on a Quantachrome Autosorb-1. X-ray Diffraction (XRD) analysis was carried out on the fresh catalysts by using a SIEMENS D5000 in the range of 10–70° with a scanning step of 0.02° using Cu Kα radiation (0.1542 nm wavelength). A high resolution scanning electron microscope (SEM) (LEO 1530) coupled to an energy dispersive X-ray spectroscope (EDXS) system was used to investigate the surface morphology and the element distributions of the reacted catalysts.

Temperature programmed reduction (TPR) was used to characterize the fresh catalysts using a Stanton–Redcroft thermogravimetric analyzer (TGA). During the TPR analysis, the fresh catalyst was heated at 20 °C $min^{-1}$ to 150 °C and held for 30 min, then heated at 10 °C $min^{-1}$ to 900 °C in an atmosphere of gas mixture containing 5% $H_2$ and 95%$N_2$ (50 ml $min^{-1}$).

Temperature-programmed oxidation (TPO) of the reacted catalysts was carried out using a Stanton–Redcroft thermogravimetric analyzer (TGA and DTG) to determine the properties of the coked carbons deposited on the reacted catalysts. About 10 mg of the reacted catalyst was heated in an atmosphere of air at 15 $min^{-1}$ to a final temperature of 800 °C, with a dwell time of 10 min. The coke amount was calculated from the weight loss of sample (300–500 °C) divided by the original sample weight.

## 3. Results and discussion

### 3.1. Characteristics of Fe–Zn/$Al_2O_3$ catalysts

The theoretical metal composition, particle size and BET surface area of the catalysts are shown in Table 1. The surface areas of Fe–Zn/$Al_2O_3$ catalysts prepared by the co-precipitation method markedly decreased from 72.8 to 11.6 $m^2$ $g^{-1}$ with the increase of Zn/Al ratio from 1:4 to 1:1 in the catalyst.

XRD patterns of Fe–Zn/$Al_2O_3$ catalysts were used to identify the species present in the catalysts as shown in Fig. 2. $FeAl_2O_4$ and $Zn(AlFe)O_4$ species were observed mainly at 31° and 36° for the XRD spectra of the catalyst with a Zn/Al ratio of 1:1. However, $Fe_2O_3$ (mainly at 24° and 33°) and $ZnAl_2O_4$ (mainly at 37°) are dominant species on all other Fe–Zn/$Al_2O_3$ catalysts. It was observed that the peak intensity of both $Fe_2O_3$ and $ZnAl_2O_4$ species increased with the change of the Zn/Al ratio from 1:4 to 1:2. Changing the Zn/Al ratio to 1:1, the spinels, i.e., $FeAl_2O_4$ and $Zn(AlFe)O_4$, were dominant on the catalysts. It indicates that the

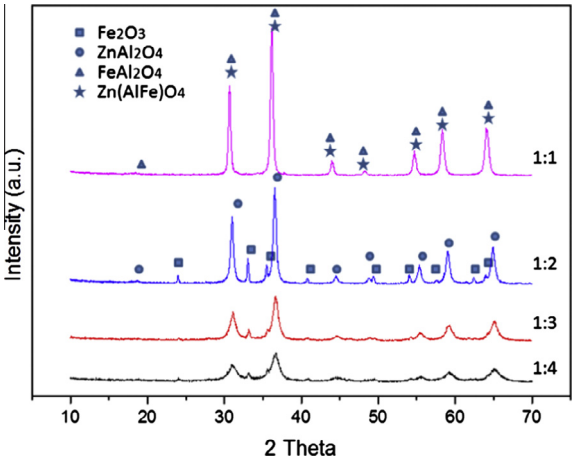


**Fig. 2.** XRD patterns of the fresh Fe–Zn/$Al_2O_3$ catalysts with Zn/Al ratios of 1:1, 1:2, 1:3 and 1:4, respectively.

formation of ferric oxide or ferric spinels in the catalysts was related to the Zn/Al ratio: ferric oxide was mainly generated on the catalysts with the Zn/Al ratio lower than 1:2; high Zn/Al ratio of 1:1 promoted the formation of ferric spinels. Zn reacted preferentially with Al to form $ZnAl_2O_4$ spinel when the Zn was at a lower amount in the catalysts. However, when the amount of Zn was increased to a certain level, i.e., the ratio of Zn/Al of around 1 in this case, Zn could react with both Fe and Al to form $FeAl_2O_4$ and $Zn(AlFe)O_4$. SEM images did not clearly show these spinels on the surface of the Fe–Zn/$Al_2O_3$catalysts as shown in Fig. 3. With the increase of the Zn content, the surfaces of the catalysts tended to be clearer and less fine grained particles were observed.

Therefore, $H_2$-TPR was used to further determine the surface species on the Fe–Zn/$Al_2O_3$ catalysts and their reducibility. As shown in Fig. 4, TPR curves for the catalysts with the Zn/Al ratios from 1:4 to 1:2 were characterized by three main reduction peaks: the first centered at around 400 °C for the reduction of ferric oxide to FeO or Fe; the second peak of FeO reduced at 600 °C; and the third one for the reduction of Fe contained spinels at 900 °C [41]. With the increase of the Zn/Al ratio to 1:1, the third peak gradually shifted from 900 °C to 800 °C, showing the increased reducibility of the compound. Spinels were mainly formed on the catalyst as confirmed by the dominant peak at a reduction temperature of 800 °C, which was also confirmed by the above XRD investigation. Only a very small amount of ferric oxide particles were located on the surface as indicated by the very weak reduction peak at 400 °C on the TPR curve and the SEM imagine of this catalyst. Zinc aluminates were non-reduced in the whole range of studied temperatures.

### 3.2. Experimental tests on Fe–Zn/$Al_2O_3$ catalysts

Gasification of the wood sawdust was carried out on Fe–Zn/$Al_2O_3$ catalysts under a water stream at 800 °C and the results are summarized in Table 2. From the calculation based on the mass

**Table 1**
Composition, size and surface areas of the Fe–Zn/$Al_2O_3$ catalysts.

| Sample | Molar ratio (Zn/Al) | Theoretical metal composition (wt.%)[a] | | | Particle size (nm)[b] | | | | BET surface area ($m^2$ $g^{-1}$) |
|---|---|---|---|---|---|---|---|---|---|
| | | Fe | Zn | $Al_2O_3$ | $FeAl_2O_4$ | $ZnFe_2O_4$ | α-$Fe_2O_3$ | $ZnAl_2O_4$ | |
| Fe–Zn/$Al_2O_3$ | 1:1- | 19.46 | 45.1 | 35.5 | – | – | – | – | 11.6 |
| Fe–Zn/$Al_2O_3$ | 1:2 | 20.0 | 31.3 | 48.7 | – | – | 46.0 | 20.3 | 28.0 |
| Fe–Zn/$Al_2O_3$ | 1:3 | 20.4 | 23.8 | 55.8 | – | – | 46.3 | 12.8 | 52.8 |
| Fe–Zn/$Al_2O_3$ | 1:4 | 20.6 | 19.3 | 60.1 | – | – | – | 12.0 | 72.8 |

[a] The theoretical metal composition was calculated via the equation M = M/(Fe + Zn + $Al_2O_3$), where M represents Fe or Zn.
[b] Particle size obtained from XRD data calculated from Scherrer's formula.

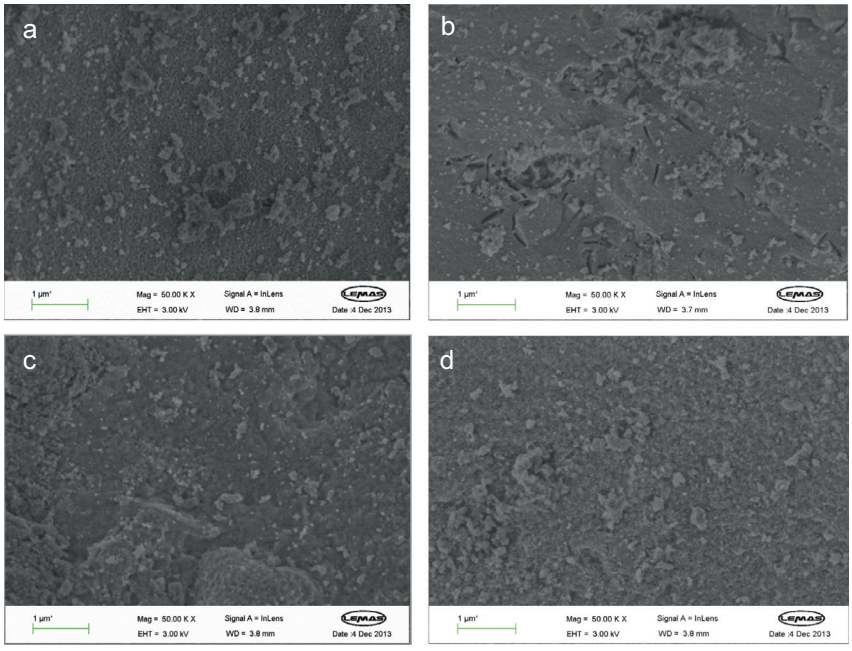


**Fig. 3.** SEM imagines of the fresh Fe–Zn/$Al_2O_3$ catalysts: (a) Zn/Al = 1:1; (b) Zn/Al = 1:2; (c) Zn/Al = 1:3; (d) Zn/Al = 1:4.

balance, it was noted that the yields of both total gas and hydrogen were clearly increased with the addition of catalysts during the thermo-chemical process. For the catalysts with ferric oxide and spinels as the main surface species (the Zn/Al ratio of the catalysts from 1:4 to 1:2), total gas yields were obtained between ca. 33 and 40 wt.% with hydrogen yields from 2.4 to 7 mmol $H_2$ $g^{-1}$ sample,

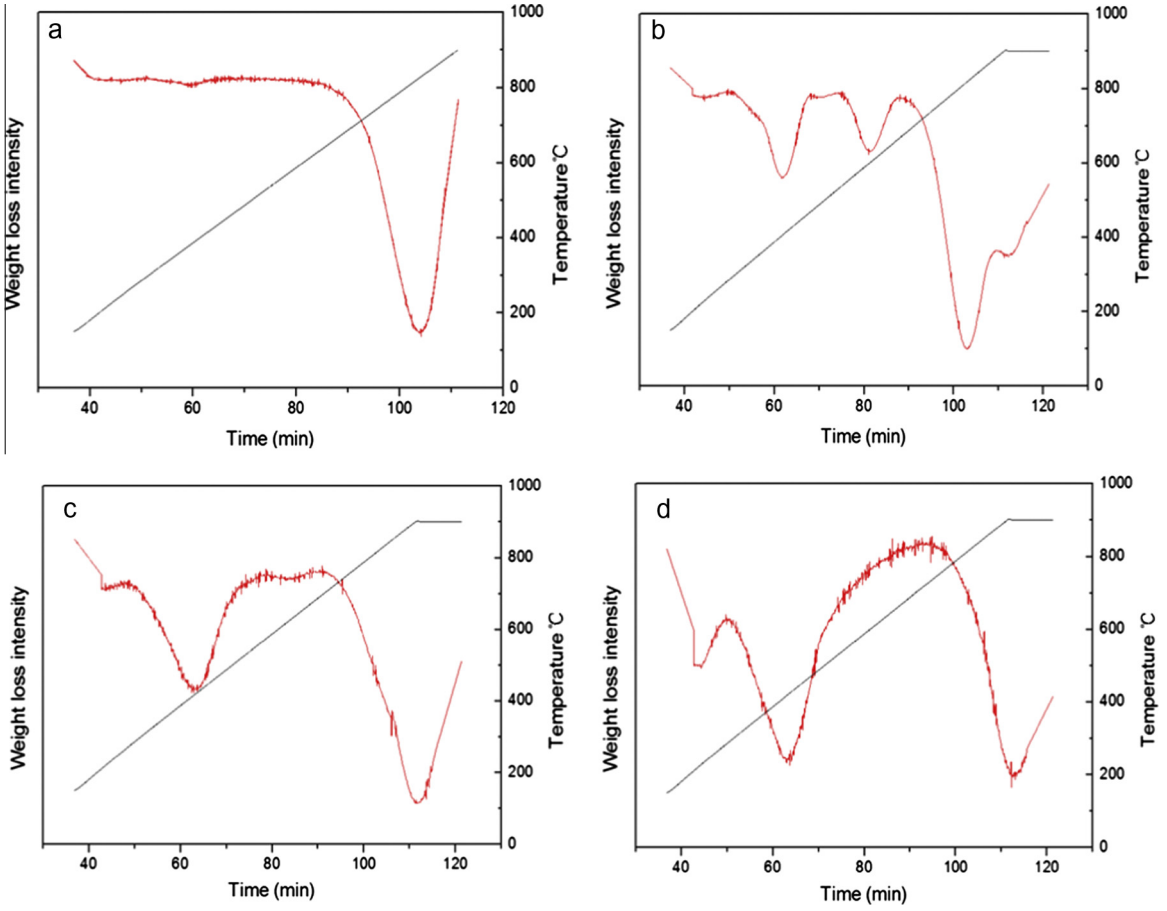


**Fig. 4.** TPR results of the Fe–Zn/$Al_2O_3$ catalysts: (a) Zn/Al = 1:1; (b) Zn/Al = 1:2; (c) Zn/Al = 1:3; (d) Zn/Al = 1:4.

respectively. While for the catalyst with only spinels as the main component, i.e., the Zn/Al ratio of 1:1, both gas and hydrogen yields were further increased up to 50 wt.% and 9.7 mmol $H_2$ $g^{-1}$ sample, respectively. Though the Fe–Zn/$Al_2O_3$ catalyst with a Zn/Al ratio of 1:1 exhibits the lowest BET surface area (6 times lower than the catalysts with a Zn/Al ratio of 1:4) in these catalysts, it contributed the highest activity in terms of hydrogen production; indicating that the BET surface area is not the key factor for the estimation of catalytic activity in this research. Therefore, the catalytic performance on the prepared catalysts was mainly dependent on their surface active sites. Catalysts with only Fe contained spinels on the catalyst surface offered the highest catalytic activity and hydrogen production during the biomass thermo-chemical processing. However, the existence of ferric oxide or FeO on the surface would reduce the reactivity of catalysts even though both species were easily reduced to active Fe for the process.

Introducing Zn into the catalysts promoted the formation of spinels and enhanced the reaction process. The change of gas composition in relation to the various Zn/Al ratios in the catalysts is summarized in Fig. 5. The hydrogen fraction in the gas maintained almost the same level at ca. 35 vol.% with the increasing of the ratio of Zn/Al from 1:4 to 1:2. Also, with the increase of Zn/Al ratio from 1:4 to 1:2, the CO fraction in the individual product gas increased from around 28 to 32 vol.%, and the $CO_2$ fraction decreased from 23 to 19 vol.%. Meanwhile, the fraction of hydrocarbon gas ($CH_4$ and $C_2$–$C_4$) produced was similar for the three catalysts. Therefore, the dry or steam reforming of small molecular weight hydrocarbons has not been influenced by the Zn/Al ratios. The WGSR of CO and water was slightly decreased with the increase of Zn. These catalysts containing both ferric oxide/FeO and Fe spinels performed similarly for hydrogen production.

The hydrogen and $CO_2$ fractions were increased to 40 and 24 vol.% respectively, with the CO fraction decreased to 24 vol.% and slightly decreased hydrocarbon fractions when the Zn/Al ratio was 1:1. The spinel only catalyst could promote hydrogen production mainly based on the WGSR as the amount of CO decreased proportionally with the increase of the amount of $CO_2$. Also, slightly improved dry reforming of hydrocarbons contributed to additional hydrogen production. The obtained gas product derived from the Fe–Zn/$Al_2O_3$ (1:1) catalyst had an optimal $H_2$/CO ratio (ca. 2), which is favored for hydrocarbon synthesis processes such as Fischer–Tropsch.

**Table 2**
Mass balance of the catalytic reforming of vapors derived from pyrolysis of sawdust on Fe–Zn/$Al_2O_3$ catalysts.

| Catalyst bed | Sand | Fe–Zn/$Al_2O_3$ | | | |
|---|---|---|---|---|---|
| | | 1:1 | 1:2 | 1:3 | 1:4 |
| Gas/biomass (wt.%) | 33.01 | 48.68 | 43.36 | 39.80 | 39.61 |
| Residue/biomass (wt.%) | 38.81 | 38.75 | 37.50 | 36.25 | 37.50 |
| Mass balance (wt.%) | 103.3 | 99.52 | 104.64 | 99.88 | 98.62 |
| $H_2$ yield (mmol $H_2$/g) | 2.40 | 9.65 | 7.25 | 6.79 | 6.59 |

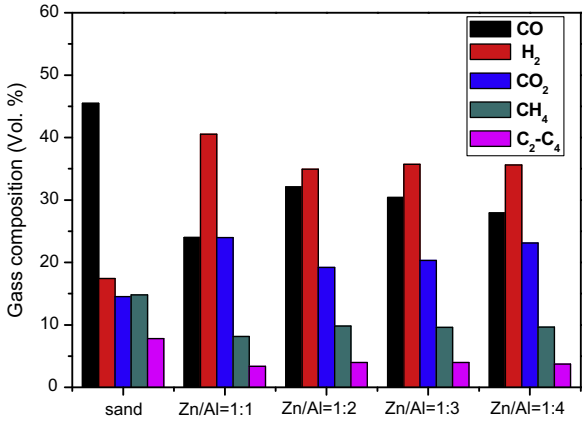


**Fig. 5.** Gas compositions and fractions from biomass thermo-chemical processing on the Fe–Zn/$Al_2O_3$ catalysts.

### 3.3. Coke formation

Section 3.2 reported that the Fe spinel dominated catalyst had much better catalytic performance compared to catalysts containing both ferric oxide/FeO and Fe spinels. Normally, better catalytic performance usually relates to heavy coke formation on the catalysts, which is a significant challenge for the development of biomass thermo-chemical processing and causes fast catalyst deactivation. In this research, the amount of coke on the various catalysts has been determined via temperature programmed oxidation (TPO) and the results are shown in Fig. 6. The amount of coke was found by subtracting the weight loss of the normal TPO results for Fe particles produced during the thermo-chemical process. Only one type of carbon was formed on the surface of the catalyst, with an oxidation peak at around 400 °C, which may be assigned to amorphous carbon, which is relatively easy to be

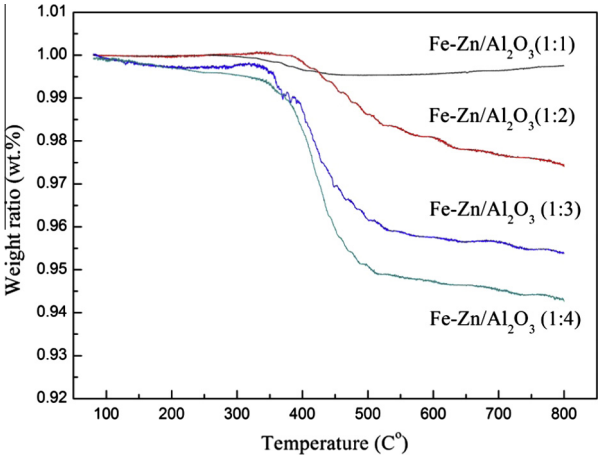


**Fig. 6.** TPO analyses of the reacted Fe–Zn/$Al_2O_3$ catalysts.

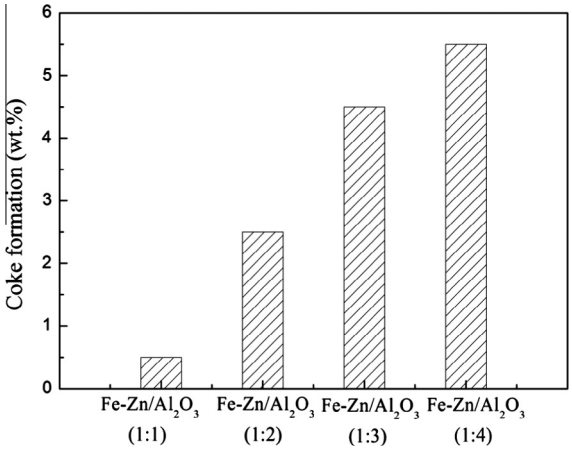


**Fig. 7.** Weight ratios of coke to the catalyst for the reacted Fe–Zn/$Al_2O_3$ catalysts.

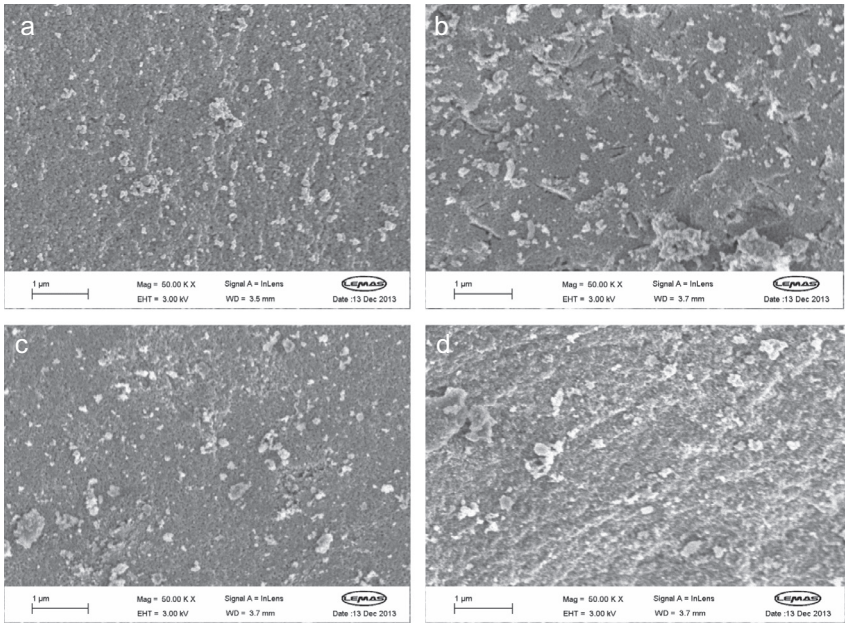


**Fig. 8.** SEM imagines of the reacted Fe–Zn/$Al_2O_3$catalysts: (a) Zn/Al = 1:1; (b) Zn/Al = 1:2; (c) Zn/Al = 1:3; (d) Zn/Al = 1:4.

removed during regeneration compared with graphite type carbons.

Detailed quantification of the coke on the catalysts was calculated based on the TPO results and are shown in Fig. 7. For the catalysts (Zn/Al ratio from 1:4 to 1:2) offering similar surface active species and catalytic performances, the amount of coke decreased from 5.5 to 2.5 wt.% with the increase of the Zn content. Adding Zn could strongly reduce the coke formation. The possible reason suggested previously is that Zn could cover the surface acid sites and thereby limit the coke deposition on the surface [8–10]. On the Fe spinel only catalyst (Zn/Al ratio of 1:1), the amount of coke was only ca. 0.5 wt.%, which is very low compared to regular catalysts used for biomass gasification [42]. Clearly, the spinel only catalyst not only offers the highest catalytic activity, but also has significant resistance to coke formation.

It was reported that Fe active sites could be dispersed atomically in the spinel structure to improve tar decomposition during gasification [36–38]. This kind of high dispersion of Fe on the spinel catalyst could overcome its shortage of the much lower surface area compared to a mixture of oxides and contribute to the higher gas production and hydrogen yield during the thermo-chemical process. It should be noted that the spinel structure is thermally stable during the reaction and is resistant to sintering as reported by previous research [43–45]. In this research SEM was used to characterize the surface morphology of all the reacted catalysts. As shown in Fig. 8, SEM did not show any obvious differences of the catalysts surface compared with the surface of the fresh catalysts (Fig. 3). It indicates that no sintering on the catalyst surface occurred during the pyrolysis catalytic reforming process and suggests high stability for the prepared catalysts.

## 4. Conclusions

In this work, the pyrolysis catalytic reforming of wood sawdust was performed on nano Fe–Zn/$Al_2O_3$ catalysts. During the thermo-chemical process, the yield of hydrogen was increasing up to a maximum with the ratio of Zn/Al from 1:4 to 1:1. The results suggest that, Zn is an efficient metal promoter for enhancing the performance of Fe active site in the reaction. Adding Zn sharply reduced the surface area of the catalysts. The higher conversion rates on these catalysts were mainly dependent on the highly dispersed Fe active sites in Fe spinels. Catalysts with dominant Fe spinel on the surface offered the highest catalytic activity and hydrogen production during the thermo-chemical process based on the enhanced water gas shift reaction and hydrocarbon dry reforming. However, the existence of ferric oxide or FeO on the surface would drop down the reactivity of catalysts even though both species were easily reduced to active Fe for the process. Introducing even small amounts of Zn could strongly improve the stability of the catalysts. As shown in SEM images, all catalysts showed ultra-high stability during the process and nearly no sintering was observed on the used catalysts. The spinel only catalyst also showed higher resistance for coke formation, only 0.5 wt.% coke was produced during the thermo-chemical conversion process and the coke was hard to be observed on the surface of the catalyst by SEM. It was demonstrated that Zn promoted Fe nanocatalysts prepared from natural, abundant and low-cost metals using a simple method have targeted catalytic properties and stability for biomass thermo-chemical processing.

## Acknowledgements

This work was supported by the International Exchange Scheme from the Royal Society (IE110273), UK, and the Early Career Research Scheme and the Materials & Structures Cluster from the University of Sydney.

## References

[1] Goltsov VA, Veziroglu TN, Goltsova LF. Hydrogen civilization of the future—a new conception of the IAHE. Int J Hydro Energy 2006;31:153–9.
[2] Ni M, Leung DYC, Leung MKH, Sumathy K. An overview of hydrogen production from biomass. Fuel Process Technol 2006;87:461–72.
[3] Wu C, Wang L, Williams PT, Shi J, Huang J. Hydrogen production from biomass gasification with Ni/MCM-41 catalysts: influence of Ni content. Appl Catal B 2011;108–109:6–13.
[4] Wang L, Weller CL, Jones DD, Hanna MA. Contemporary issues in thermal gasification of biomass and its application to electricity and fuel production. Biomass Bioenergy 2008;32:573–81.
[5] Sutton D, Kelleher B, Ross JRH. Review of literature on catalysts for biomass gasification. Fuel Process Technol 2001;73:155–73.
[6] Mortensen PM, Grunwaldt JD, Jensen PA, Knudsen KG, Jensen AD. A review of catalytic upgrading of bio-oil to engine fuels. Appl Catal A 2011;407:1–19.

[7] Olaleye AK, Adedayo KJ, Wu C, Nahil MA, Wang M, Williams PT. Experimental study, dynamic modelling, validation and analysis of hydrogen production from biomass pyrolysis/gasification of biomass in a two-stage fixed bed reaction system. Fuel 2014;137:364–74.
[8] Tanksale A, Beltramini JN, Lu GM. A review of catalytic hydrogen production processes from biomass. Renew Sustain Energy Rev 2010;14:166–82.
[9] Parthasarathy P, Narayanan KS. Hydrogen production from steam gasification of biomass: influence of process parameters on hydrogen yield – a review. Renew Energy 2014;66:570–9.
[10] Font Palma C. Modelling of tar formation and evolution for biomass gasification: a review. Appl Energy 2013;111:129–41.
[11] Shen Y, Yoshikawa K. Recent progresses in catalytic tar elimination during biomass gasification or pyrolysis—a review. Renew Sustain Energy Rev 2013;21:371–92.
[12] Chan FL, Tanksale A. Review of recent developments in Ni-based catalysts for biomass gasification. Renew Sustain Energy Rev 2014;38:428–38.
[13] Chen Y-G, Tomishige K, Yokoyama K, Fujimoto K. Catalytic performance and catalyst structure of nickel–magnesia catalysts for $CO_2$ reforming of methane. J Catal 1999;184:479–90.
[14] Tomishige K, Chen Y-G, Fujimoto K. Studies on carbon deposition in $CO_2$ reforming of $CH_4$ over nickel–magnesia solid solution catalysts. J Catal 1999;181:91–103.
[15] Lemonidou AA, Goula MA, Vasalos IA. Carbon dioxide reforming of methane over nickel calcium aluminate catalysts – effect of preparation method. Catal Today 1998;46:175–83.
[16] Choong CKS, Huang L, Zhong Z, Lin J, Hong L, Chen L. Effect of calcium addition on catalytic ethanol steam reforming of $Ni/Al_2O_3$: II. Acidity/basicity, water adsorption and catalytic activity. Appl Catal A 2011;407:155–62.
[17] Dias JAC, Assaf JM. Influence of calcium content in $Ni/CaO/\gamma\text{-}Al_2O_3$ catalysts for $CO_2$-reforming of methane. Catal Today 2003;85:59–68.
[18] Agrell J, Boutonnet M, Fierro JLG. Production of hydrogen from methanol over binary Cu/ZnO catalysts: Part II. Catalytic activity and reaction pathways. Appl Catal A 2003;253:213–23.
[19] Turco M, Bagnasco G, Costantino U, Marmottini F, Montanari T, Ramis G, et al. Production of hydrogen from oxidative steam reforming of methanol: II. Catalytic activity and reaction mechanism on $Cu/ZnO/Al_2O_3$ hydrotalcite-derived catalysts. J Catal 2004;228:56–65.
[20] Lu W, Lu G, Liu X, Guo Y, Wang J, Guo Y. Effects of support and modifiers on catalytic performance of zinc oxide for hydrogenation of methyl benzoate to benzaldehyde. Mater Chem Phys 2003;82:120–7.
[21] Barroso MN, Gomez MF, Arrúa LA, Abello MC. Hydrogen production by ethanol reforming over NiZnAl catalysts. Appl Catal A 2006;304:116–23.
[22] Chen J, Qiao Y, Li Y. Promoting effects of doping ZnO into coprecipitated $Ni–Al_2O_3$ catalyst on methane decomposition to hydrogen and carbon nanofibers. Appl Catal A 2008;337:148–54.
[23] Chen J, Qiao Y, Li Y. Modification of Ni state to promote the stability of $Ni–Al_2O_3$ catalyst in methane decomposition to produce hydrogen and carbon nanofibers. J Solid State Chem 2012;191:107–13.
[24] Buitrago-Sierra R, Ruiz-Martínez J, Serrano-Ruiz JC, Rodríguez-Reinoso F, Sepúlveda-Escribano A. Ethanol steam reforming on $Ni/Al_2O_3$ catalysts: effect of the addition of Zn and Pt. J Colloid Interface Sci 2012;383:148–54.
[25] Shishido T, Yamamoto Y, Morioka H, Takehira K. Production of hydrogen from methanol over Cu/ZnO and $Cu/ZnO/Al_2O_3$ catalysts prepared by homogeneous precipitation: steam reforming and oxidative steam reforming. J Mol Catal A 2007;268:185–94.
[26] Yang M, Men Y, Li S, Chen G. Hydrogen production by steam reforming of dimethyl ether over $ZnO–Al_2O_3$ bi-functional catalyst. Int J Hydro Energy 2012;37:8360–9.
[27] Farahani BV, Rajabi FH, Bahmani M, Ghelichkhani M, Sahebdelfar S. Influence of precipitation conditions on precursor particle size distribution and activity of Cu/ZnO methanol synthesis catalyst. Appl Catal A 2014;482:237–44.
[28] Ni M, Leung DYC, Leung MKH. A review on reforming bio-ethanol for hydrogen production. Int J Hydro Energy 2007;32:3238–47.
[29] Castro Luna AE, Iriarte ME. Carbon dioxide reforming of methane over a metal modified $Ni–Al_2O_3$ catalyst. Appl Catal A 2008;343:10–5.
[30] Chen L, Choong CKS, Zhong Z, Huang L, Wang Z, Lin J. Support and alloy effects on activity and product selectivity for ethanol steam reforming over supported nickel cobalt catalysts. Int J Hydrogen Energy 2012;37:16321–32.
[31] Reshetenko TV, Avdeeva LB, Khassin AA, Kustova GN, Ushakov VA, Moroz EM, et al. Coprecipitated iron-containing catalysts ($Fe–Al_2O_3$, $Fe–Co–Al_2O_3$, $Fe–Ni–Al_2O_3$) for methane decomposition at moderate temperatures: I. Genesis of calcined and reduced catalysts. Appl Catal A 2004;268:127–38.
[32] Reshetenko TV, Avdeeva LB, Ushakov VA, Moroz EM, Shmakov AN, Kriventsov VV, et al. Coprecipitated iron-containing catalysts ($Fe–Al_2O_3$, $Fe–Co–Al_2O_3$, $Fe–Ni–Al_2O_3$) for methane decomposition at moderate temperatures: Part II. Evolution of the catalysts in reaction. Appl Catal A 2004;270:87–99.
[33] Wang L, Li D, Koike M, Koso S, Nakagawa Y, Xu Y, et al. Catalytic performance and characterization of Ni–Fe catalysts for the steam reforming of tar from biomass pyrolysis to synthesis gas. Appl Catal A 2011;392:248–55.
[34] Nordgreen T, Liliedahl T, Sjöström K. Metallic iron as a tar breakdown catalyst related to atmospheric fluidised bed gasification of biomass. Fuel 2006;85:689–94.
[35] Świerczyński D, Libs S, Courson C, Kiennemann A. Steam reforming of tar from a biomass thermo-chemical process over Ni/olivine catalyst using toluene as a model compound. Appl Catal B 2007;74:211–22.
[36] Devi L, Ptasinski KJ, Janssen FJJG. Pretreated olivine as tar removal catalyst for biomass gasifiers: investigation using naphthalene as model biomass tar. Fuel Process Technol 2005;86:707–30.
[37] Devi L, Ptasinski KJ, Janssen FJJG. A review of the primary measures for tar elimination in biomass thermo-chemical processes. Biomass Bioenergy 2003;24:125–40.
[38] Kuhn JN, Zhao Z, Felix LG, Slimane RB, Choi CW, Ozkan US. Olivine catalysts for methane- and tar-steam reforming. Appl Catal B 2008;81:14–26.
[39] Duman G, Watanabe T, Uddin MA, Yanik J. Steam gasification of safflower seed cake and catalytic tar decomposition over ceria modified iron oxide catalysts. Fuel Process Technol 2014;126:276–83.
[40] Venugopal A, Scurrell MS. Low temperature reductive pretreatment of $Au/Fe_2O_3$ catalysts, TPR/TPO studies and behaviour in the water–gas shift reaction. Appl Catal A 2004;258:241–9.
[41] Liang M, Kang W, Xie K. Comparison of reduction behavior of $Fe_2O_3$, ZnO and $ZnFe_2O_4$ by TPR technique. J Nat Gas Chem 2009;18:110–3.
[42] Nishikawa J, Miyazawa T, Nakamura K, et al. Promoting effect of Pt addition to $Ni/CeO_2/Al_2O_3$ catalyst for steam gasification of biomass. Catal Commun 2008;9:195–201.
[43] Hull S, Trawczyński J. Steam reforming of ethanol on zinc containing catalysts with spinel structure. Int J Hydrogen Energy 2014;39:4259–65.
[44] Muroyama H, Nakase R, Matsui T, Eguchi K. Ethanol steam reforming over Ni-based spinel oxide. Int J Hydrogen Energy 2010;35:1575–81.
[45] Sehested J, Gelten JAP, Remediakis IN, Bengaard H, Nørskov JK. Sintering of nickel steam-reforming catalysts: effects of temperature and steam and hydrogen pressures. J Catal 2004;223:432–43.